Belief Propagation Based Joint Probabilistic Data Association for Multipath-Assisted Indoor Navigation and Tracking

Erik Leitinger*, Florian Meyer†, Paul Meissner*, Klaus Witrisal*, and Franz Hlawatsch‡

*Graz University of Technology, Graz, Austria ({erik.leitinger,paul.meissner,witrisal}@tugraz.at)
†Centre for Maritime Research and Experimentation, La Spezia, Italy (florian.meyer@cmre.nato.int)
‡TU Wien, Vienna, Austria (fhlawats@nt.tuwien.ac.at)

***Abstract*—We apply joint probabilistic data association (JPDA) to multipath-assisted indoor navigation and tracking (MINT). In MINT, position-related information in multipath components (MPCs) is exploited to increase the accuracy and robustness of indoor tracking. Conventional MINT algorithms are based on deterministic data association and perform a global nearest-neighbor "hard" association of MPC-related delays with the room geometry. In such a setup, incorrect associations may lead to severe tracking errors and to divergence of the Bayesian filter. Here, we propose a JPDA-MINT algorithm that is able to handle difficult situations where MPC delays overlap and data association is ambiguous. The algorithm is based on a recently introduced loopy belief propagation scheme that performs probabilistic data association jointly with agent state estimation, scales well in all relevant systems parameters, and has a very low computational complexity. Using data from an ultra-wideband indoor measurement campaign, we demonstrate that the proposed JPDA-MINT algorithm is highly accurate and more robust than the conventional MINT algorithms based on deterministic data association.**

I. Introduction

The multipath-assisted indoor navigation and tracking (MINT) approach exploits position-related information in multipath components (MPCs) that can be associated with the local geometry [1]–[4]. It thus turns multipath propagation from an impairment into an advantage. Using ultra-wideband (UWB) transmit signals, specular MPCs are estimated from the received signals and used for positioning and tracking. This is accomplished by associating the estimated MPC delays with delays corresponding to the geometric distance between the mobile agent and a physical anchor or a corresponding virtual source referred to as *virtual anchor* (VA) [5]. Thus, each MPC corresponds to a physical anchor or to a corresponding VA. The VA positions are mirror images of the positions of the physical anchors as illustrated in Fig. 1a; they are obtained by using a-priori knowledge of the floor plan or a simultaneous-localization-and-mapping algorithm [6]. In the example shown in Fig. 1a, a mobile agent at position $\mathbf{p}_n$ is tracked using the estimated MPC delays associated with the delays corresponding to the distances between the mobile agent and two physical anchors at positions $\mathbf{a}_1^{(1)}$ and $\mathbf{a}_1^{(2)}$ and two VAs at positions $\mathbf{a}_2^{(2)}$ and $\mathbf{a}_3^{(2)}$.

A critical step of MINT is the data association between the MPC delays estimated from the received signal and the anchors (both physical anchors and VAs[1]) representing prior knowledge on the room geometry. In our previous work [1]–[4], we employed the Hungarian or Munkres algorithm [7] based on the optimal sub-pattern assignment (OSPA) metric [8] to find the optimal association between MPC delays and anchors. A major drawback of such deterministic and "hard" data association methods is that wrong assignments can lead

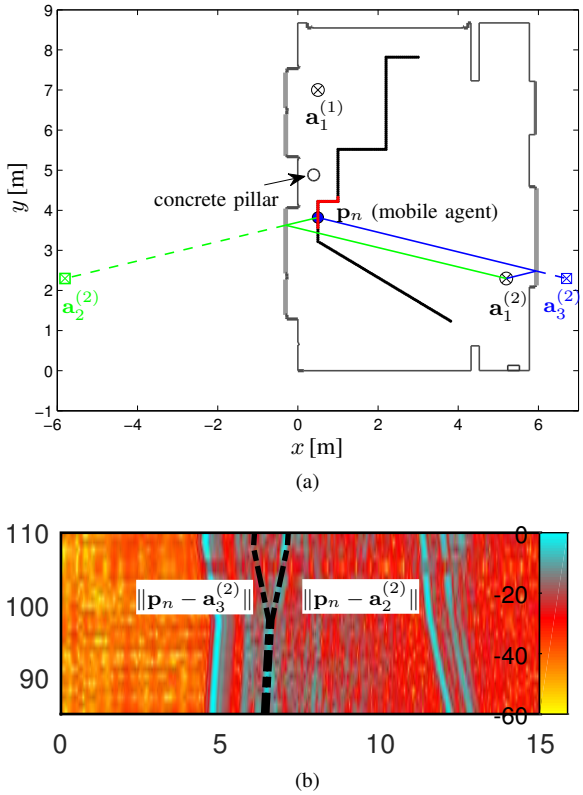

Fig. 1. (a) Floor plan of the evaluation scenario (cf. Section V). A mobile agent at position $\mathbf{p}_n$ (blue dot) is tracked (thick black line) using the estimated MPC delays associated with two physical anchors at positions $\mathbf{a}_1^{(1)}$ and $\mathbf{a}_1^{(2)}$ and VAs at positions $\mathbf{a}_2^{(2)}$ and $\mathbf{a}_3^{(2)}$. (b) Absolute value of the signal (function of discrete time n) received at the mobile agent and transmitted by the physical anchor at $\mathbf{a}_1^{(2)}$. The signal is displayed for different mobile agent positions along the red part of the trajectory shown in (a); for each position the signal is shown along the delay axis scaled by the speed of light c and therefore corresponding to the distance d. The two dashed-dotted black lines indicate the delays corresponding to the distances between the agent and the VAs at $\mathbf{a}_2^{(2)}$ and at $\mathbf{a}_3^{(2)}$.

This work was supported in part by the Austrian Research Promotion Agency (FFG) within the project REFlex (grant 845630) and in part by the Austrian Science Fund (FWF) under grant P27370-N30.

[1]Hereafter, both physical and virtual anchors will be generically referred to as "anchors".

to divergence of the subsequent Bayesian tracking filter [9]. Especially in situations where the MPC-anchor associations are ambiguous, deterministic data association is problematic. Fig. 1a shows such a path-overlap situation, where it is not clear whether an estimated MPC delay should be associated with the delay corresponding to the distance between the mobile agent and the VA at $\mathbf{a}_2^{(2)}$ or the delay corresponding to the distance between the mobile agent and the VA at $\mathbf{a}_3^{(2)}$ (these delays are indicated in Fig. 1b by black dashed-dotted lines).

To overcome such robustness issues, we introduce a joint probabilistic data association (JPDA) method for MINT. The conventional JPDA filter [9] is a well-established technique for multitarget tracking in the presence of data association uncertainty. The JPDA algorithm avoids hard association decisions, which results in increased tracking accuracy and robustness. However, it is unsuitable for multiple physical anchors, scales poorly in the number of anchors (physical anchor with according VAs), and suffers from a detrimental effect known as track coalescence [10]. Here, we adapt a recently introduced belief propagation (BP) message passing algorithm for JPDA and agent tracking [11] to MINT. Based on a factor graph framework and using a hybrid formulation of data association introduced in [12], the proposed JPDA-MINT algorithm jointly performs JPDA and agent tracking by means of loopy BP [13]. The computational complexity of the algorithm scales only quadratically with the number of anchors, which improves on the cubic scaling exhibited by the Munkres data association algorithm employed in conventional MINT algorithms. Using real data from a UWB indoor measurement campaign, we demonstrate that the proposed algorithm is highly accurate and more robust than the conventional MINT algorithm based on deterministic data association.

The paper is organized as follows: Section II discusses the basic principles of MINT and MPC parameter estimation. Section III introduces the system model and provides a statistical formulation. In Section IV, the proposed BP algorithm is described. Section V presents experimental results.

II. Principles of MINT

In this section, we review the basic concept of MINT and discuss the estimation of the MPC parameters.

A. Signal Model

During time step n, a baseband UWB signal $s(t)$ is transmitted from the j-th physical anchor located at position $\mathbf{a}_1^{(j)} \in \mathbb{R}^2$, with $j \in \{1, \dots, J\}$, to a mobile agent at position $\mathbf{p}_n \in \mathbb{R}^2$. The corresponding received signal is modeled as [4]

$$r_n^{(j)}(t) = \sum_{k=1}^{K_n^{(j)}} \alpha_{k,n}^{(j)} s\big(t - \tau_{k,n}^{(j)}\big) + \big(s * \nu_n^{(j)}\big)(t) + w(t). \quad (1)$$

Here, the first term describes the sum of $K_n^{(j)}$ deterministic MPCs with complex amplitudes $\alpha_{k,n}^{(j)}$ and delays $\tau_{k,n}^{(j)}$, where $k \in \big\{1, \dots, K_n^{(j)}\big\}$. The delays $\tau_{k,n}^{(j)}$ correspond to the distances between the agent and the j-th physical anchor (for $k = 1$) or the VAs of the j-th physical anchor (for $k \in \big\{2, \dots, K_n^{(j)}\big\}$). Thus, $\tau_{k,n}^{(j)} = \big\|\mathbf{p}_n - \mathbf{a}_k^{(j)}\big\|/c$, where $\mathbf{a}_k^{(j)} \in \mathbb{R}^2$ is the position of the respective (physical or virtual) anchor and c is the speed of light. The energy of the transmitted signal $s(t)$ is assumed to be normalized to one. The second term in (1) denotes the convolution of $s(t)$ with the diffuse-multipath function $\nu_n^{(j)}(t)$, which is modeled as a non-stationary zero-mean Gaussian random process. For the diffuse multipath, we assume uncorrelated scattering along the delay axis τ, hence the auto-correlation function of $\nu_n^{(j)}(t)$ is given by $\mathbb{E}_\nu\big\{\nu_n^{(j)}(\tau)\nu_n^{(j)*}(u)\big\} = S_{\nu,n}^{(j)}(\tau)\delta(\tau - u)$, where $S_{\nu,n}^{(j)}(\tau)$ is the power delay profile of the diffuse multipath at agent position $\mathbf{p}_n$. The diffuse multipath process $\nu_n^{(j)}(t)$ is assumed to be quasi-stationary in the spatial domain, which means that $S_{\nu,n}^{(j)}(\tau)$ does not change in the vicinity of $\mathbf{p}_n$ [14]. Note that the diffuse multipath component interferes with the useful position-related information. The last term in (1), $w(t)$, is additive white Gaussian noise with double-sided power spectral density $N_0/2$.

B. MPC Parameter Estimation

The MPC delays at agent position $\mathbf{p}_n$ are estimated recursive by a least-squares approximation of the received signal [2]. The estimate of the m-th MPC delay is calculated as

$$\hat{\tau}_{m,n}^{(j)} = \arg\min_{\tau} \int_0^T \big|r_n^{(j)}(t) - \hat{r}_{n,m-1}^{(j)}(t) - \hat{\alpha}(\tau)s(t-\tau)\big|^2 \mathrm{d}t, \quad (2)$$

where T is the measurement duration, $\hat{r}_{n,m-1}^{(j)}(t)$ is a template signal containing all MPCs up to the $(m-1)$-th, and

$$\hat{\alpha}(\tau) = \int_0^T \big[r_n^{(j)}(t) - \hat{r}_{n,m-1}^{(j)}(t)\big] s^*(t-\tau)\mathrm{d}t. \quad (3)$$

The template signal is formed as

$$\hat{r}_{n,m-1}^{(j)}(t) = \sum_{m'=1}^{m-1} \hat{\alpha}_{m',n}^{(j)} s\big(t - \hat{\tau}_{m',n}^{(j)}\big),$$

where $\hat{\alpha}_{m,n}^{(j)}$ is an estimate of the m-th amplitude that is obtained as $\hat{\alpha}_{m,n}^{(j)} = \hat{\alpha}\big(\hat{\tau}_{m,n}^{(j)}\big)$. Alternating between (2) and (3), the algorithm recursively estimates the MPC parameters $\tau_{m,n}^{(j)}$ and $\alpha_{m,n}^{(j)}$ until a predefined number M of MPCs is reached. The template signal is initialized with $\hat{r}_{n,0}^{(j)}(t) = 0$.

The estimated delays are scaled by the speed of light c, i.e., $y_{m,n}^{(j)} = c\hat{\tau}_{m,n}^{(j)}$, with $m \in \{1, \dots, M\}$, and used as noisy distance measurements in the proposed JPDA-MINT algorithm. Furthermore, in a real-world MINT system, the amplitude estimates $\hat{\alpha}_{m,n}^{(j)}$ (after being associated with the k-th anchor) are fed into a higher-level, non-Bayesian algorithm that determines the signal-to-interference-plus-noise power ratio between the useful deterministic MPC and the diffuse-multipath plus noise. This power ratio is related to the measurement variances $\sigma_{m,n}^{(j)2}$ (see [2], [4] for details).

III. System Model and Statistical Formulation

The state of the mobile agent at time step n is $\mathbf{x}_n = [\mathbf{p}_n^{\mathrm{T}}, \mathbf{v}_n^{\mathrm{T}}]^{\mathrm{T}}$, where $\mathbf{v}_n$ is the velocity. The state evolves over time n according to a prescribed state transition probability density function (PDF) $f(\mathbf{x}_n|\mathbf{x}_{n-1})$.

A. Target-oriented Association Vector and Global Likelihood Function

The MPC distances described in Section II-B are subject to a data association uncertainty, i.e., it is not known which measurement $y_{m,n}^{(j)}$ in $\mathbf{y}_n^{(j)} \triangleq \big[y_{1,n}^{(j)}, \ldots, y_{M,n}^{(j)}\big]^{\mathrm{T}}$ originated from which anchor k at position $\mathbf{a}_k^{(j)}$, and it is also possible that a measurement $y_{m,n}^{(j)}$ did not originate from any anchor (false alarm, clutter) or that an anchor did not give rise to any measurement (missed detection). The probability that an anchor is detected is assumed to be constant and denoted by P_{d}. Possible associations at time n are described by the $K_n^{(j)}$-dimensional random vector $\mathbf{c}_n^{(j)} = \big[c_{1,n}^{(j)}, \ldots, c_{K_n^{(j)},n}^{(j)}\big]^{\mathrm{T}}$, whose k-th entry is defined as

$$c_{k,n}^{(j)} = \begin{cases} m \in \{1, \ldots, M\}, & \text{at time } n, \text{ anchor } k \\ & \text{generates mesurement } y_{m,n}^{(j)} \\ 0, & \text{at time } n, \text{ anchor } k \\ & \text{does not generate any} \\ & \text{measurement.} \end{cases}$$

We also define $\mathbf{c}_n \triangleq \big[\mathbf{c}_n^{(1)\,\mathrm{T}}, \ldots, \mathbf{c}_n^{(J)\,\mathrm{T}}\big]^{\mathrm{T}}$. The distribution of false alarm measurements $f_{\mathrm{FA}}\big(y_{m,n}^{(j)}\big)$ is modeled as uniform on the region of interest, i.e., the distance interval $[0, cT]$.

Let us stack the distance measurement vectors $\mathbf{y}_n^{(j)}$, $j \in \{1, \ldots, J\}$ obtained from all the signal transmissions and MPC estimation procedures into the vector $\mathbf{y}_n \triangleq \big[\mathbf{y}_n^{(1)\,\mathrm{T}}, \ldots, \mathbf{y}_n^{(J)\,\mathrm{T}}\big]^{\mathrm{T}}$. The statistical dependence of the distance measurement vector $\mathbf{y}_n$ on the agent state vector $\mathbf{x}_n$ and the association $\mathbf{c}_n$ is described by the *global likelihood function* $f(\mathbf{y}_n|\mathbf{x}_n, \mathbf{c}_n)$. Under commonly used assumptions about the statistics of the measurements [1], [9], [15], the global likelihood function factors as

$$f(\mathbf{y}_n|\mathbf{x}_n, \mathbf{c}_n) = \prod_{j=1}^{J} \left(\prod_{m=1}^{M} f_{\mathrm{FA}}\big(y_{m,n}^{(j)}\big) \right) \times \prod_{k \in \mathcal{Q}(\mathbf{x}_n, \mathbf{c}_n^{(j)})} \frac{f\Big(y_{c_{k,n}^{(j)},n}^{(j)} \Big| \mathbf{x}_n; \mathbf{a}_k^{(j)}, \sigma_{k,n}^{(j)\,2}\Big)}{f_{\mathrm{FA}}\Big(y_{c_{k,n}^{(j)},n}^{(j)}\Big)}, \quad (4)$$

where $\mathcal{Q}\big(\mathbf{x}_n, \mathbf{c}_n^{(j)}\big)$ is the subset of MPCs $k \in \big\{1, \ldots, K_n^{(j)}\big\}$ for which $c_{k,n}^{(j)} \neq 0$ and $\sigma_{c_{k,n}^{(j)},n}^{(j)\,2}$ is the variance of $y_{c_{k,n}^{(j)},n}^{(j)}$. Since $\mathbf{y}_n$ is observed and thus fixed, (4) can be written as

$$f(\mathbf{y}_n|\mathbf{x}_n, \mathbf{c}_n) \propto \prod_{j=1}^{J} \prod_{k=1}^{K_n^{(j)}} g\big(\mathbf{x}_n, c_{k,n}^{(j)}; \mathbf{y}_n^{(j)}\big), \quad (5)$$

where

$$g\big(\mathbf{x}_n, c_{k,n}^{(j)}; \mathbf{y}_n^{(j)}\big) = \begin{cases} \dfrac{f\Big(y_{c_{k,n}^{(j)},n}^{(j)} \Big| \mathbf{x}_n; \mathbf{a}_k^{(j)}, \sigma_{k,n}^{(j)\,2}\Big)}{f_{\mathrm{FA}}\Big(y_{c_{k,n}^{(j)},n}^{(j)}\Big)}, & c_{k,n}^{(j)} \neq 0 \\ 1, & \text{otherwise.} \end{cases}$$

Here, the likelihood function $f\Big(y_{c_{k,n}^{(j)},n}^{(j)} \Big| \mathbf{x}_n; \mathbf{a}_k^{(j)}, \sigma_{k,n}^{(j)\,2}\Big)$ is related to a noisy measurement of the distance between agent position $\mathbf{p}_n$ and anchor position $\mathbf{a}_k^{(j)}$. This measurement is modeled as

$$y_{c_{k,n}^{(j)},n}^{(j)} = \|\mathbf{p}_n - \mathbf{a}_k^{(j)}\| + v_{k,n}^{(j)},$$

where $v_{k,n}^{(j)}$ is zero-mean Gaussian noise with variance $\sigma_{c_{k,n}^{(j)},n}^{(j)\,2}$, assumed independent across j, k and n.

The prior probability mass function (PMF) of the association vector $\mathbf{c}_n^{(j)}$ is given by [9], [15]

$$p\big(\mathbf{c}_n^{(j)}\big) \propto \tilde{\psi}\big(\mathbf{c}_n^{(j)}\big) \prod_{k=1}^{K_n^{(j)}} \varphi\big(c_{k,n}^{(j)}\big), \quad (6)$$

where $\tilde{\psi}\big(\mathbf{c}_n^{(j)}\big)$ and $\varphi\big(c_{k,n}^{(j)}\big)$ are defined as follows. We assume that at any time n, each anchor can generate at most one measurement, and each measurement can be generated by at most one anchor [1], [9], [15]. These exclusion assumptions are "encoded" in $p\big(\mathbf{c}_n^{(j)}\big)$ by setting

$$\tilde{\psi}\big(\mathbf{c}_n^{(j)}\big) = \begin{cases} 0, & \exists k, l \in \{1, \ldots, K_n^{(j)}\} \text{ s.t. } c_{k,n}^{(j)} = c_{l,n}^{(j)} \neq 0 \\ 1, & \text{otherwise.} \end{cases} \quad (7)$$

By modeling the number of false alarms by a Poisson distribution with mean μ, the remaining factors in (6) are given by [9], [15]

$$\varphi\big(c_{k,n}^{(j)}\big) = \begin{cases} P_{\mathrm{d}}/\mu, & c_{k,n}^{(j)} \in \{1, \ldots, M\} \\ 1 - P_{\mathrm{d}}, & c_{k,n}^{(j)} = 0. \end{cases}$$

B. Measurement-oriented Association Vector

As previously proposed in [11], we introduce a *measurement-oriented association vector* $\mathbf{b}_n^{(j)} = \big[b_{1,n}^{(j)}, \ldots, b_{M,n}^{(j)}\big]^{\mathrm{T}}$ with

$$b_{m,n}^{(j)} = \begin{cases} k \in \big\{1, \ldots, K_n^{(j)}\big\}, & \text{measurement } y_{m,n}^{(j)} \text{ is} \\ & \text{generated by anchor } k \\ 0, & \text{measurement } y_{m,n}^{(j)} \text{ is not} \\ & \text{generated by any anchor.} \end{cases}$$

We also define $\mathbf{b}_n \triangleq \big[\mathbf{b}_n^{(1)\,\mathrm{T}}, \ldots, \mathbf{b}_n^{(J)\,\mathrm{T}}\big]^{\mathrm{T}}$. Following [11], the exclusion indicator function (7) can be replaced by

$$\psi\big(\mathbf{c}_n^{(j)}, \mathbf{b}_n^{(j)}\big) = \prod_{k=1}^{K_n^{(j)}} \prod_{m=1}^{M} \Psi\big(c_{k,n}^{(j)}, b_{m,n}^{(j)}\big) \quad (8)$$

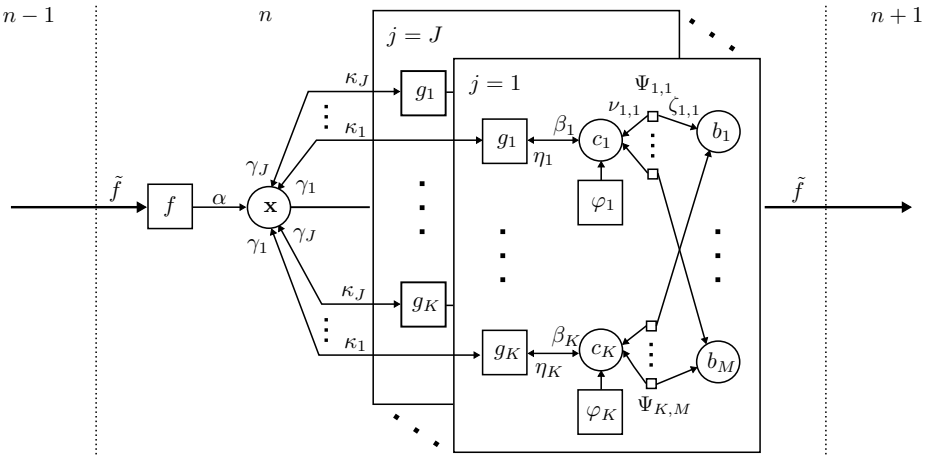

Fig. 2. Factor graph corresponding to the factorization in (13). The following short notations are used: $\mathbf{x} \triangleq \mathbf{x}_n$, $f \triangleq f(\mathbf{x}_n|\mathbf{x}_{n-1})$, $g_k \triangleq g\big(\mathbf{x}_n, c_{k,n}^{(j)}; \mathbf{y}_n^{(j)}\big)$, $\alpha \triangleq \alpha(\mathbf{x}_n)$, $b_m \triangleq b_{m,n}^{(j)}$, $c_k \triangleq c_{k,n}^{(j)}$, $\tilde{f} \triangleq \tilde{f}(\mathbf{x}_n)$, $\Psi_{k,m} \triangleq \Psi\big(c_{k,n}^{(j)}, b_{m,n}^{(j)}\big)$, $\beta_k \triangleq \beta\big(c_{k,n}^{(j)}\big)$, $\eta_k \triangleq \eta\big(c_{k,n}^{(j)}\big)$, $\varphi_k \triangleq \varphi\big(c_{k,n}^{(j)}\big)$, $\nu_{m,k} \triangleq \nu_{m\to k}^{(p)}\big(c_{k,n}^{(j)}\big)$, $\zeta_{k,m} \triangleq \zeta_{k\to m}^{(p)}\big(b_{m,n}^{(j)}\big)$, $\kappa_j \triangleq \kappa_{\to j}^{(q)}(\mathbf{x}_n)$, and $\gamma_j \triangleq \gamma_{j\to}^{(q)}(\mathbf{x}_n)$.

with

$$\Psi\big(c_{k,n}^{(j)}, b_{m,n}^{(j)}\big) = \begin{cases} 0, & c_{k,n}^{(j)} = m,\ b_{m,n}^{(j)} \neq k \\ & \quad \text{or } b_{m,n}^{(j)} = k,\ c_{k,n}^{(j)} \neq m \\ 1, & \text{otherwise.} \end{cases} \tag{9}$$

Equations (8) and (9) are equivalent to the exclusion relation in (7). Note that $\mathbf{b}_n^{(j)}$ can be constructed from $\mathbf{c}_n^{(j)}$ and vice versa. The joint PMF of $\mathbf{c}_n^{(j)}$ and $\mathbf{b}_n^{(j)}$ is given as (cf. (6))

$$\begin{aligned} p\big(\mathbf{c}_n^{(j)}, \mathbf{b}_n^{(j)}\big) &\propto \psi\big(\mathbf{c}_n^{(j)}, \mathbf{b}_n^{(j)}\big) \prod_{k=1}^{K_n^{(j)}} \varphi\big(c_{k,n}^{(j)}\big) \\ &= \prod_{k=1}^{K_n^{(j)}} \varphi\big(c_{k,n}^{(j)}\big) \prod_{m=1}^{M} \Psi\big(c_{k,n}^{(j)}, b_{m,n}^{(j)}\big). \end{aligned} \tag{10}$$

C. Problem Statement

The problem addressed in the Bayesian part of MINT is estimation of the agent state $\mathbf{x}_n$ from all the past and present measurements of all the anchors $j \in \{1, \ldots, J\}$, i.e., from the total measurement vector $\mathbf{y} \triangleq \big[\mathbf{y}_1^{\mathrm{T}}, \ldots, \mathbf{y}_n^{\mathrm{T}}\big]^{\mathrm{T}}$, and from the room geometry represented by the anchor positions $\mathbf{a}_k^{(j)}$, $k \in \big\{1, \ldots, K_n^{(j)}\big\}$, $j \in \{1, \ldots, J\}$. More specifically, we will develop an approximate calculation of the minimum mean-square error (MMSE) estimator [16]

$$\hat{\mathbf{x}}_n^{\mathrm{MMSE}} \triangleq \int \mathbf{x}_n\, f(\mathbf{x}_n|\mathbf{y})\, \mathrm{d}\mathbf{x}_n\,. \tag{11}$$

In addition, the higher-level algorithm that determines the variance $\sigma_{k,n}^{(j)\,2}$ corresponding to each anchor, requires knowledge of the most probable MPC-to-anchor association. This is obtained by means of an approximation of the maximum a posterior (MAP) detector [17]

$$\hat{c}_{k,n}^{(j)\,\mathrm{MAP}} \triangleq \underset{c_{k,n}^{(j)} \in \{1,\ldots,M\}}{\arg\max}\ p\big(c_{k,n}^{(j)}|\mathbf{y}\big). \tag{12}$$

These calculations will be based on approximate calculations of the marginal posterior PDFs $f(\mathbf{x}_n|\mathbf{y})$ and the marginal posterior PMFs $p\big(c_{k,n}^{(j)}|\mathbf{y}\big)$ involved in (11) and (12), respectively, by means of an efficient BP message passing algorithm.

IV. BP Message Passing For JPDA-MINT

In this section, we develop the proposed BP-based JPDA-MINT method.

A. Factorization of the Joint Posterior PDF

Let $\mathbf{x} \triangleq \big[\mathbf{x}_0^{\mathrm{T}}, \ldots, \mathbf{x}_n^{\mathrm{T}}\big]^{\mathrm{T}}$, $\mathbf{c} \triangleq \big[\mathbf{c}_1^{\mathrm{T}}, \ldots, \mathbf{c}_n^{\mathrm{T}}\big]^{\mathrm{T}}$, and $\mathbf{b} \triangleq \big[\mathbf{b}_1^{\mathrm{T}}, \ldots, \mathbf{b}_n^{\mathrm{T}}\big]^{\mathrm{T}}$. Using Bayes' rule and common independence assumptions [1], [9], [15], the joint posterior PDF $f(\mathbf{x}, \mathbf{c}, \mathbf{b}|\mathbf{y})$ can be expressed up to a constant factor as

$$\begin{aligned} f(\mathbf{x}, \mathbf{c}, \mathbf{b}|\mathbf{y}) &\propto f(\mathbf{y}|\mathbf{x}, \mathbf{c}, \mathbf{b})\, f(\mathbf{x}, \mathbf{c}, \mathbf{b}) \\ &= f(\mathbf{y}|\mathbf{x}, \mathbf{c})\, f(\mathbf{x})\, p(\mathbf{c}, \mathbf{b}) \\ &= f(\mathbf{x}_0) \prod_{n'=1}^{n} f(\mathbf{x}_{n'}|\mathbf{x}_{n'-1})\, p(\mathbf{c}_{n'}, \mathbf{b}_{n'}) \\ &\quad \times f(\mathbf{y}_{n'}|\mathbf{x}_{n'}, \mathbf{c}_{n'}) \\ &\propto f(\mathbf{x}_0) \prod_{n'=1}^{n} f(\mathbf{x}_n|\mathbf{x}_{n'-1}) \prod_{j=1}^{J} \prod_{k=1}^{K_{n'}^{(j)}} \varphi\big(c_{k,n'}^{(j)}\big) \\ &\quad \times g\big(\mathbf{x}_{n'}, c_{k,n'}^{(j)}; \mathbf{y}_{n'}^{(j)}\big) \prod_{m=1}^{M} \Psi\big(c_{k,n'}^{(j)}, b_{m,n'}^{(j)}\big)\,, \end{aligned} \tag{13}$$

where (5) and (10) have been used. This factorization of the joint posterior PDF can be represented by the factor graph shown in Fig. 2. By running BP message passing on this factor graph, approximations of $f(\mathbf{x}_n|\mathbf{y})$ and $p\big(c_{k,n}^{(j)}|\mathbf{y}\big)$ can be obtained.

B. BP Message Passing Algorithm

The proposed BP message passing algorithm is an adaptation of the algorithm introduced in [11] to the factor graph in Fig. 2. The algorithm executes an outer iteration loop for information fusion from different physical anchors and an inner loop for iterative data association. At time n, first a prediction step is performed, yielding

$$\alpha(\mathbf{x}_n) = \int f(\mathbf{x}_n|\mathbf{x}_{n-1})\tilde{f}^{(Q)}(\mathbf{x}_{n-1})\mathrm{d}\mathbf{x}_{n-1},$$

where $\tilde{f}^{(Q)}(\mathbf{x}_{n-1})$ is the final result of the outer iteration loop at time $n-1$. The outer iteration loop (with iteration index $q \in \{1,\dots,Q\}$) is performed in parallel for all anchors $k \in \mathcal{K}_n^{(j)} \triangleq \{1,\dots,K_n^{(j)}\}$ and all physical anchors $j \in \mathcal{J} \triangleq \{1,\dots,J\}$. The q-th iteration comprises the following steps:

1) Measurement evaluation:

$$\beta^{(q)}\big(c_{k,n}^{(j)}\big) = \int g\big(\mathbf{x}_n, c_{k,n}^{(j)}; \mathbf{y}_n^{(j)}\big)\kappa_{\to j}^{(q-1)}(\mathbf{x}_n)\mathrm{d}\mathbf{x}_n.$$

2) Iterative data association (inner loop):

$$\eta^{(q)}\big(c_{k,n}^{(j)}\big) = \varphi\big(c_{k,n}^{(j)}\big)\prod_{m\in\mathcal{M}}\nu_{m\to k}^{(q,P)}\big(c_{k,n}^{(j)}\big),$$

where $\mathcal{M} \triangleq \{1,\dots,M\}$ and $\nu_{m\to k}^{(q,P)}(c_{k,n}^{(j)})$ is the result of the inner BP message passing iteration loop. The inner loop (iteration index $p \in \{1,\dots,P\}$) is performed for all measurements $m \in \mathcal{M}$ by executing the following steps:

$$\nu_{m\to k}^{(q,p)}\big(c_{k,n}^{(j)}\big) = \sum_{b_{m,n}^{(j)}}\Psi\big(c_{k,n}^{(j)}, b_{m,n}^{(j)}\big)\prod_{k'\in\mathcal{K}_n^{(j)}\setminus\{k\}}\zeta_{k'\to m}^{(q,p-1)}\big(b_{m,n}^{(j)}\big)$$

and

$$\zeta_{k\to m}^{(q,p)}\big(b_{m,n}^{(j)}\big) = \sum_{c_{k,n}^{(j)}}\beta^{(q)}\big(c_{k,n}^{(j)}\big)\varphi\big(c_{k,n}^{(j)}\big)\Psi\big(c_{k,n}^{(j)}, b_{m,n}^{(j)}\big) \times\prod_{m'\in\mathcal{M}\setminus\{m\}}\nu_{m'\to k}^{(q,p)}\big(c_{k,n}^{(j)}\big).$$

This inner iteration loop is initialized with

$$\zeta_{k\to m}^{(q,0)}\big(b_{m,n}^{(j)}\big) = \sum_{c_{k,n}^{(j)}}\beta^{(q)}\big(c_{k,n}^{(j)}\big)\varphi\big(c_{k,n}^{(j)}\big)\Psi\big(c_{k,n}^{(j)}, b_{m,n}^{(j)}\big).$$

3) Measurement update:

$$\gamma_{j\to}^{(q)}(\mathbf{x}_n) = \sum_{c_{k,n}^{(j)}} g\big(\mathbf{x}_n, c_{k,n}^{(j)}; \mathbf{y}_n^{(j)}\big)\eta^{(q)}\big(c_{k,n}^{(j)}\big).$$

4) Outer loop update:

$$\kappa_{\to j}^{(q)}(\mathbf{x}_n) = \alpha(\mathbf{x}_n)\prod_{j'\in\mathcal{J}\setminus\{j\}}\gamma_{j'\to}^{(q)}(\mathbf{x}_n).$$

The outer loop iteration is initialized with $\kappa_{\to j}^{(0)}(\mathbf{x}_n) = \alpha(\mathbf{x}_n)$, which is provided by the prediction step. Finally, after $q = Q$ iterations, the belief $\tilde{f}^{(Q)}(\mathbf{x}_n)$ approximating the marginal posterior PDF $f(\mathbf{x}_n|\mathbf{y})$ is calculated as

$$\tilde{f}^{(Q)}(\mathbf{x}_n) \propto \alpha(\mathbf{x}_n)\prod_{j\in\mathcal{J}}\gamma_{j\to}^{(Q)}(\mathbf{x}_n).$$

Similarly, the beliefs $\tilde{p}^{(Q,P)}\big(c_{k,n}^{(j)}\big)$ approximating the marginal posterior PMFs $p\big(c_{k,n}^{(j)}|\mathbf{y}\big)$ are calculated as

$$\tilde{p}^{(Q,P)}\big(c_{k,n}^{(j)}\big) = \beta_{\to}^{(Q)}\big(c_{k,n}^{(j)}\big)\varphi\big(c_{k,n}^{(j)}\big)\prod_{m\in\mathcal{M}}\nu_{m\to k}^{(Q,P)}\big(c_{k,n}^{(j)}\big).$$

The beliefs $\tilde{f}^{(Q)}(\mathbf{x}_n)$ and $\tilde{p}^{(Q,P)}\big(c_{k,n}^{(j)}\big)$ are substituted for $f(\mathbf{x}_n|\mathbf{y})$ in (11) and for $p\big(c_{k,n}^{(j)}|\mathbf{y}\big)$ in (12), respectively.

V. Experimental Results

We compare the performance of the proposed JDPA-MINT algorithm with that of the conventional MINT method using the Munkres algorithm for deterministic OSPA-based data association [2], [3]. This performance comparison is based on real UWB measurements.

A. Measurement Setup

The measurements are taken from the seminar room scenario of the MeasureMINT database [18]. They correspond to five parallel trajectories, each consisting of 1000 agent positions with a 1 cm spacing. Fig. 1a shows one of these trajectories. At each agent position, UWB measurements of the channel between the agent and two physical anchors at positions $\mathbf{a}_1^{(1)} = [0.5, 7]^{\mathrm{T}}$ and $\mathbf{a}_1^{(2)} = [5.2, 3.2]^{\mathrm{T}}$ are available. The measurements were performed using an M-sequence correlative channel sounder with frequency range $3-10$ GHz, i.e., approximately the FCC frequency range. On the anchor and agent sides, dipole-like antennas made of Eurocent coins were used. These antennas have an approximately uniform radiation pattern in the azimuth plane and zeros in the directions of floor and ceiling. Within the total measured band, we selected the actual signal band using filtering with a root raised cosine pulse $s(t)$ with a roll-off-factor of 0.5 and two-sided bandwidth of 3 GHz at a center frequency of $f_{\mathrm{c}} = 7$ GHz.

B. Experimental Setup

The agent moves according to a linear Gaussian constant-velocity motion model [19], i.e.,

$$\mathbf{x}_n = \begin{bmatrix}1 & 0 & \Delta T & 0\\ 0 & 1 & 0 & \Delta T\\ 0 & 0 & 1 & 0\\ 0 & 0 & 0 & 1\end{bmatrix}\mathbf{x}_{n-1} + \begin{bmatrix}\Delta T^2/2 & 0\\ 0 & \Delta T^2/2\\ \Delta T & 0\\ 0 & \Delta T\end{bmatrix}\mathbf{w}_n,$$

where $\mathbf{x}_n = [\mathbf{p}_n^{\mathrm{T}}, \mathbf{v}_n^{\mathrm{T}}]^{\mathrm{T}}$ as before. The driving noise $\mathbf{w}_n$ is independent across n, zero-mean, and Gaussian with covariance matrix $\mathbf{R}_w = \sigma_{\mathrm{w}}^2\mathbf{I}$. We chose $\sigma_{\mathrm{w}}^2 = 0.001\,\mathrm{m/s^2}$ and $\Delta T = 1$ s.

For each of the two physical anchors, we calculated the positions of $K_n^{(j)} \approx 300$ VAs using the floor plan shown in Fig. 1a and the known physical anchor positions $\mathbf{a}_1^{(1)}$ and $\mathbf{a}_1^{(2)}$. Because we did not restrict the VAs to those visible at the agent position [2], many VAs can lead to ambiguous associations

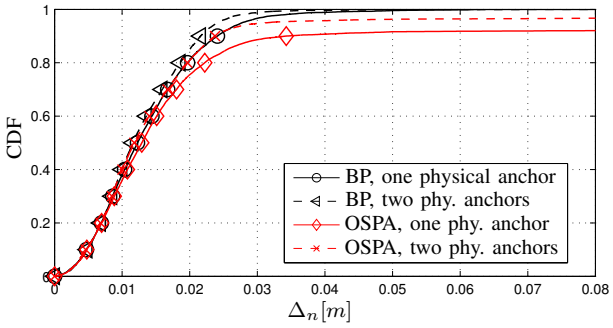

Fig. 3. CDF of the position error of MINT using deterministic OSPA-based data association (red lines) and the proposed JPDA data association (black lines). Solid lines represent the case of only one physical anchor at position $\mathbf{a}_1^{(2)}$; dashed lines represent the case of two physical anchors at positions $\mathbf{a}_1^{(1)}$ and $\mathbf{a}_1^{(2)}$.

with MPCs. This is a challenging scenario for the deterministic data association performed by conventional MINT methods.

We estimated $M = 20$ MPCs. The range variances $\sigma_{k,n}^{(j)\,2}$ corresponding to the nonzero $c_{k,n}^{(j)}$ were determined by a higher-level algorithm that uses estimates of the complex MPC amplitudes of the last 30 time steps (see [2] for details). Anchors whose range variances $\sigma_{k,n}^{(j)\,2}$ is higher than a threshold $\sigma_{d,\max}^2$ are excluded from data association. Thereby, the number of VAs per physical anchor is reduced to $K_n^{(j)} \approx 20$. The false alarm PDF $f_{\mathrm{FA}}\big(y_{m,n}^{(j)}\big)$ is uniform on $[0\,\mathrm{m}, 40\,\mathrm{m}]$. The mean number of false alarms ($c_{k,n}^{(j)} = 0$) is $\mu = 5$. The detection probability $P_\mathrm{d} = 0.9$.

Both of the considered methods use a sequential importance resampling particle filter implementation with $N = 10000$ particles. The number of outer-loop iterations is $Q = 1$ and the number of inner-loop iterations is limited by the termination condition $\big[\sum_k \sum_m \big(\nu_{m\to k}^{(q,p)}(c_{k,n}^{(j)}) - \nu_{m\to k}^{(q,p-1)}(c_{k,n}^{(j)})\big)^2\big]^{1/2} < 10^{-6}$. The agent state belief $\hat{f}^{(Q)}(\mathbf{x}_n)$ is represented by a set of particles and weights $\big\{\big(\mathbf{x}_n^{(i)}, w_n^{(i)}\big)\big\}_{i=1}^N$, from which an approximation of the MMSE estimate $\hat{\mathbf{x}}_n^{\mathrm{MMSE}}$ (see (11)) is calculated as $\hat{\mathbf{x}}_n = [\hat{\mathbf{p}}_n^{\mathrm{T}}, \hat{\mathbf{v}}_n^{\mathrm{T}}]^{\mathrm{T}} = \sum_{i=1}^N w_n^{(i)} \mathbf{x}_n^{(i)}$.

C. Performance Results

Fig. 3 shows the empirical cumulative distribution function (CDF) of the agent position error $\Delta_n \triangleq \|\mathbf{p}_n - \hat{\mathbf{p}}_n\|$ along the five trajectories with 1000 agent positions, calculated from ten simulation runs. The red lines illustrate the performance of the conventional MINT algorithm and the black lines that of the JPDA-MINT algorithm. It can be seen that the overall performance of the proposed JPDA-MINT algorithm is better than that of the conventional MINT algorithm. The performance degradation of the conventional MINT algorithm can be explained by geometric room symmetries along the agent trajectory, which lead to ambiguities in data association, i.e., to many competing MPC-anchor association pairs. Hence, there is a high probability that the deterministic data association algorithm results in a suboptimal MPC-anchor association, which may cause the subsequent Bayesian filter to diverge. In contrast, the proposed JPDA-MINT jointly performs data association and tracking and therefore is able to solve difficult data association tasks.

VI. Conclusions

We proposed a method for multipath-assisted navigation and tracking (MINT) that simultaneously performs joint probabilistic data association (JPDA) and agent tracking by means of loopy belief propagation message passing. The proposed JPDA-MINT algorithm shows excellent performance and robustness against divergence in difficult situations where estimated MPC delays overlap and their association with the physical and virtual anchors is ambiguous. At the same time, the computational complexity of the proposed JPDA-MINT method is smaller than that of the conventional MINT method.

References

[1] P. Meissner, "Multipath-assisted indoor positioning," Ph.D. dissertation, Graz University of Technology, 2014.

[2] P. Meissner, E. Leitinger, and K. Witrisal, "UWB for robust indoor tracking: Weighting of multipath components for efficient estimation," *IEEE Wireless Commun. Lett.*, vol. 3, no. 5, pp. 501–504, Oct. 2014.

[3] E. Leitinger, "Cognitive indoor positioning and tracking using multipath channel information," Ph.D. dissertation, Graz University of Technology, 2016.

[4] E. Leitinger, P. Meissner, C. Rudisser, G. Dumphart, and K. Witrisal, "Evaluation of position-related information in multipath components for indoor positioning," *IEEE J. Sel. Areas Commun.*, vol. 33, no. 11, pp. 2313–2328, Nov. 2015.

[5] J. Borish, "Extension of the image model to arbitrary polyhedra," *J. Acoust. Soc. Am.*, vol. 75, no. 6, pp. 1827–1827, March 1984.

[6] E. Leitinger, P. Meissner, M. Lafer, and K. Witrisal, "Simultaneous localization and mapping using multipath channel information," in *Proc. IEEE International Conference on Communication Workshop (ICCW)*, London, UK, Jun. 2015, pp. 754–760.

[7] J. Munkres, "Algorithms for the assignment and transportation problems," *Journal of the Society for Industrial and Applied Mathematics*, vol. 5, no. 1, pp. 32–38, March 1957.

[8] D. Schuhmacher, B.-T. Vo, and B.-N. Vo, "A consistent metric for performance evaluation of multi-object filters," *IEEE Trans. Signal Process.*, vol. 56, no. 8, pp. 3447–3457, Aug. 2008.

[9] Y. Bar-Shalom and X.-R. Li, *Multitarget-Multisensor Tracking: Principles and Techniques*. Storrs, CT: Yaakov Bar-Shalom, 1995.

[10] L. Svensson, D. Svensson, M. Guerriero, and P. Willett, "Set JPDA filter for multitarget tracking," *IEEE Trans. Signal Process.*, vol. 59, no. 10, pp. 4677–4691, Oct. 2011.

[11] F. Meyer, P. Braca, P. Willett, and F. Hlawatsch, "Scalable multitarget tracking using multiple sensors: A belief propagation approach," in *Proc. FUSION-15*, Washington D.C., USA, Jul. 2015, pp. 1778–1785.

[12] J. Williams and R. Lau, "Approximate evaluation of marginal association probabilities with belief propagation," *IEEE Trans. Aerosp. Electron. Syst.*, vol. 50, no. 4, pp. 2942–2959, Oct. 2014.

[13] F. Kschischang, B. Frey, and H.-A. Loeliger, "Factor graphs and the sum-product algorithm," *IEEE Trans. Inf. Theory*, vol. 47, no. 2, pp. 498–519, Feb 2001.

[14] A. Molisch, "Ultra-wide-band propagation channels," *Proc. IEEE*, vol. 97, no. 2, pp. 353–371, Feb. 2009.

[15] J. Vermaak, S. J. Godsill, and P. Perez, "Monte Carlo filtering for multi target tracking and data association," *IEEE Trans. Aerosp. Electron. Syst.*, vol. 41, no. 1, pp. 309–332, Jan. 2005.

[16] S. M. Kay, *Fundamentals of Statistical Signal Processing: Estimation Theory*. Upper Saddle River, NJ: Prentice-Hall, 1993.

[17] ——, *Fundamentals of Statistical Signal Processing: Detection Theory*. Upper Saddle River, NJ: Prentice-Hall, 1998.

[18] P. Meissner, E. Leitinger, M. Lafer, and K. Witrisal, "MeasureMINT UWB database," 2013. [Online]. Available: www.spsc.tugraz.at/tools/UWBmeasurements

[19] X. Li and V. Jilkov, "Survey of maneuvering target tracking. Part I. Dynamic models," *IEEE Trans. Aerosp. Electron. Syst.*, vol. 39, no. 4, pp. 1333–1364, Oct 2003.